Brazilian Journal
of Chemical
Engineering

ISSN 0104-6632
Printed in Brazil
www.abeq.org.br/bjche

Vol. 25, No. 02, pp. 375 - 387, April - June, 2008

KINETICS OF BARIUM SULPHATE REACTION CRYSTALLIZATION IN CRYSTALLIZERS WITH INTERNAL CIRCULATION

J. Koralewska[1], K. Piotrowski[2*], B. Wierzbowska[1] and A. Matynia[1]

[1]Wrocław University of Technology, Faculty of Chemistry, Phone +(48) (71) 320-3497,
Fax +(48) (71) 328-0425, Wybrzeże Wyspiańskiego 27, 50-370, Wrocław, Poland.
E-mail: joanna.koralewska@pwr.wroc.pl, E-mail: andrzej.matynia@pwr.wroc.pl,
E-mail: boguslawa.wierzbowska@pwr.wroc.pl
[2]Silesian University of Technology, Department of Chemical & Process Engineering,
Phone/Fax +(48) (32) 237-1461, ks. M. Strzody 7, 44-101, Gliwice, Poland.
E-mail: krzysztof.piotrowski@polsl.pl

(Received: February 22, 2007 ; Accepted: July 29, 2007)

Abstract - Kinetic calculation results describing the observed nucleation and growth rates of barium sulphate crystals precipitated in an integrated reaction-crystallization process in a barium sulphate-ammonium chloride-water system are presented and analyzed. The scope of experiments included two continuous model DTM-type crystallizers (Draft Tube Magma) with internal circulation of the suspension forced by a liquid jet-pump device responsible for stable and intensive enough ascending/descending flow of $BaSO_4$ crystal magma in a mixing chamber. For comparison purposes the experimental data corresponding to a continuous DT (Draft Tube) crystallizer with propeller agitator are presented and discussed. The various types of laboratory crystallizers used were fed with concentrated water solution of barium chloride (of 10 or 24 mass %) and - in a stoichiometric proportion - crystalline ammonium sulphate, assuming isothermal (348 K) and hydrodynamic (average residence time of suspension in a crystallizer: 900 s) process conditions. The observed nucleation and growth rates of barium sulphate crystals were estimated on the basis of crystal size distributions (CSDs) using convenient calculation scheme derived for an MSMPR (Mixed Suspension Mixed Product Removal) model approach. Considering the experimental population density distribution courses, a size-dependent growth (SDG) phenomenon was taken into account in the kinetic calculations. Five SDG kinetic models recommended in the accessible literature were used for kinetic parameter values estimation. It was proved statistically, that Rojkowski's two SDG models (hyperbolic and exponential) best suit for our own experimental data description. The experimental data presented can be practically applied for improving the constructions of liquid jet-pump DTM crystallizers recommended for reaction crystallization of sparingly soluble inorganic salts (especially for high concentrations of reaction substrates) in the modern industrial-scale technologies.
Keywords: Barium sulphate; Precipitation; Barium chloride; Ammonium sulphate; Reaction crystallization kinetics; Size-dependent growth (SDG); DTM MSMPR crystallizer; DT MSMPR crystallizer; Liquid jet pump.

INTRODUCTION

Taking successful advantage of mass crystallization processes on various scales is possible owing to integration of precisely selected crystallizer construction, rational arrangement of its interior and optimal selection of technological parameter values. In the majority of modern continuous crystallizer constructions a convenient method to regulate the supersaturation level in a working volume (to prevent the appearance of undesirable, uncontrolled concentration gradient) proved to be an inner

*To whom correspondence should be addressed

circulation of suspension inside the apparatus. This liquid/suspension flow produces uniformity of temperature and concentration within the working volume and creates a suspended state of growing crystals and prevents their inconvenient agglomeration (Mullin, 1993; Myerson, 1993; Mersmann, 1995). Circulation of suspension inside the hydraulic system of the apparatus reduces the formation of incrustation considerably as well as prevents fast clogging of all important crystallizer elements. The constructions with some simple geometrical element responsible for improvement of circulation and no classification effects within the solid phase are usually classified as DTM MSMPR (Draft Tube Magma, Mixed Suspension Mixed Product Removal) type crystallizers. The device responsible for adjustable forced circulation of suspension inside the vessel is usually an agitator (of one of a variety of constructions) or a circulation pump. On the basis of long-term observations it can be concluded that in large-scale industrial installations the pumps consume considerable amounts of electrical energy. Moreover, their rotors can negatively affect the quality of the solid phase (destruction of surface, breakage, intensification of attrition, etc.). On the other hand, application of an agitator requires a precise balance of the shaft coupled with the selection of an appropriate bearing system. Additionally, in the case of utilizing the crystallizer bottom as the shaft's input location, reliable packing becomes extremely important. A considerably simpler device, both from a construction and a utilization point of view, to produce effective circulation of suspension inside the vessel, although still rarely used in industrial and laboratory practice, is a jet-pump device (Rojkowski and Synowiec, 1991; Matynia, 1997).

The lack of internal movable elements, thus considerably reducing mechanical destruction of the crystal phase; a simple construction; and the possibility of producing properly shaped crystals coupled with relatively low energy consumption are the main advantages of crystallizers with a liquid jet-pump device. Manual or fully automatic adjustment of its working conditions (e.g. optimal ejection degree) is possible with relatively easily available valves. If necessary, it is possible to replace a whole jet-pump device or an integral part (e.g. feeding nozzle) by another with more convenient geometrical proportions.

The original constructions of jet-pump crystallizers have until now been successfully applied in various processes of mass crystallization from solutions, including complex reaction crystallization technologies (Matynia, 1997). The practical applicability of these constructions in reaction crystallization of sparingly soluble salts, calcium (hydroxyapatite – HAP) and magnesium/ ammonium (struvite – MAP) phosphates (Matynia et al. 2005a) as well as barium sulphate (Koralewska et al., 2006a, Koralewska et al., 2006b) and others, has actually been tested.

In the work presented the kinetic data corresponding to continuous reaction crystallization of $BaSO_4$ in two laboratory crystallizers equipped with a jet-pump device with different directions of suspension circulation (later denoted as DTM↑ and DTM↓ crystallizers; see Fig. 1a and Fig. 1b) and – for comparison purposes – to that in a "reference," conventional crystallizer equipped with a propeller agitator (later denoted as DT – Draft Tube – crystallizer; see Fig. 1c) are presented and discussed in detail. The test stand equipment operation was precisely controlled by means of a PC computer. Nucleation and growth rates of $BaSO_4$ crystals were estimated on the basis of crystal size distributions (CSDs), owing to their characteristic curves observed by taking into account the size-dependent growth (SDG) kinetic models.

Separation of barium sulphate from water solution is a typical mass crystallization process preceded by a strictly integrated chemical (here, very fast ionic) reaction of sparingly soluble salt precipitation ($BaSO_4$ solubility product ($K_{sp} = a_{Ba^{2+}} a_{SO_4^{2-}}$) is 1.1×10^{-10} (mol dm^{-3})^2). Running this complex process in a controlled way enables one to provide the optimal conditions for the course of the chemical reaction, nucleation and crystal growth (Nielsen, 1964; Nývlt et al., 1985; Söhnel and Garside, 1993; Mersmann, 1995), thus making it possible to obtain the quality required for the product's further usage or postprocessing.

Both in scientific work and precisely controlled reaction crystallization experiments, barium sulphate is very often used as a model chemical compound for precipitation, appropriate for analysis. Thus, one has at his or her disposal a great number of data from the literature in this area and relatively extensive research documentation and kinetic data concerning its precipitation under various technological conditions (e.g. Matynia et al., 2001). In a presented research study the barium ions (after $BaCl_2$ dissociation) were precipitated in a sulphate form after addition of crystalline ammonium sulphate(VI). The barium chloride concentration in the crystallizer feeding solution was 10 or 24 mass %. Thus, the $BaSO_4$ precipitation conditions in the crystallizers

can be regarded as extreme. However, application of a highly concentrated water solution of $BaCl_2$ as well as crystalline $(NH_4)_2SO_4$ as a second reagent resulted from the necessity of design-oriented utilization of the results (e.g. process data, resulting kinetic relationships, suggestions on use of liquid jet-pump DTM crystallizers) in original, proecological and modern technology for utilization of toxic solid wastes after processes of metal heat treatment (so-called postquenching salts) by chemical neutralization (Matynia, 2002; Matynia et al., 2004).

EXPERIMENTAL

Setup and Procedure

The simplified schemes of crystallizer construction used in the experiments on continuous reaction crystallization of barium sulphate presented in Fig. 1 are:

- Fig. 1a – a DTM↑ type crystallizer with a liquid jet-pump. The feeding nozzle of a jet-pump was situated in the apparatus bottom profile, thus providing an ascending flow of suspension in a mixing chamber (working volume $V_w = 1.2$ dm^3).
- Fig. 1b – a DTM↓ type crystallizer with a liquid jet-pump. The feeding nozzle of a jet-pump was situated below a upper liquid level, thus providing a descending flow of suspension in a mixing chamber ($V_w = 1.2$ dm^3).
- Fig. 1c – a classical DT-type "reference" crystallizer with a three-paddle propeller agitator, providing a descending flow of suspension in a circulation profile ($V_w = 0.6$ dm^3).

A scheme of the laboratory test stand with the exemplary DTM↑ laboratory-scale crystallizer selected is presented in Fig. 2. Operation, control and recording of the measurement data were performed by the integrated automatic system controlled by a PC computer. The details of constructional elements within the individual crystallizers and main dimensions of their individual elements as well as the work regime and characteristics of operating conditions (including hydrodynamic ones) are presented in Koralewska et al. (2006a), Koralewska et al. (2006b) and Matynia et al. (2005a).

All experimental tests were run assuming a minimal value of unit power of a jet-pump feeding stream, thus resulting in a possibly minimal intensity of suspension circulation in the model crystallizers: DTM↑ crystallizer – 0.63 and 1.2 W kg^{-1}, DTM↓ crystallizer – 0.43 and 0.91 W kg^{-1} for $[BaCl_2]_{RM}$ = 10 and 24 mass %, respectively. In the case of the DT crystallizer the minimum number of revolutions of the agitator was 7 s^{-1}.

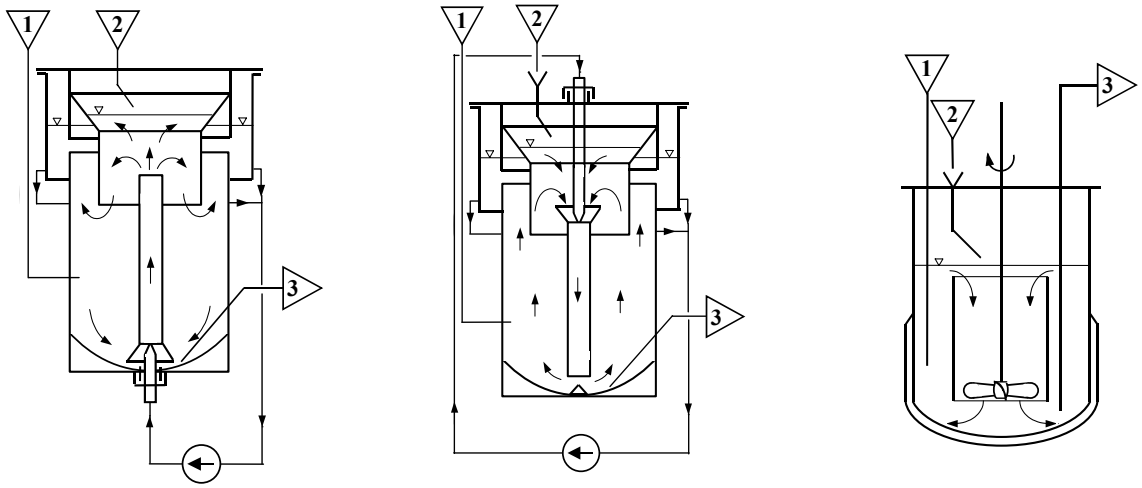

Figure 1: Schemes of the crystallizers under study: (a) - DTM↑ type crystallizer with a liquid jet-pump of ascending suspension flow in a mixing chamber: (b) - DTM↓ type crystallizer with a liquid jet-pump of descending suspension flow in a mixing chamber: (c) - DT-type crystallizer with a propeller agitator of descending suspension flow in a draft tube element.

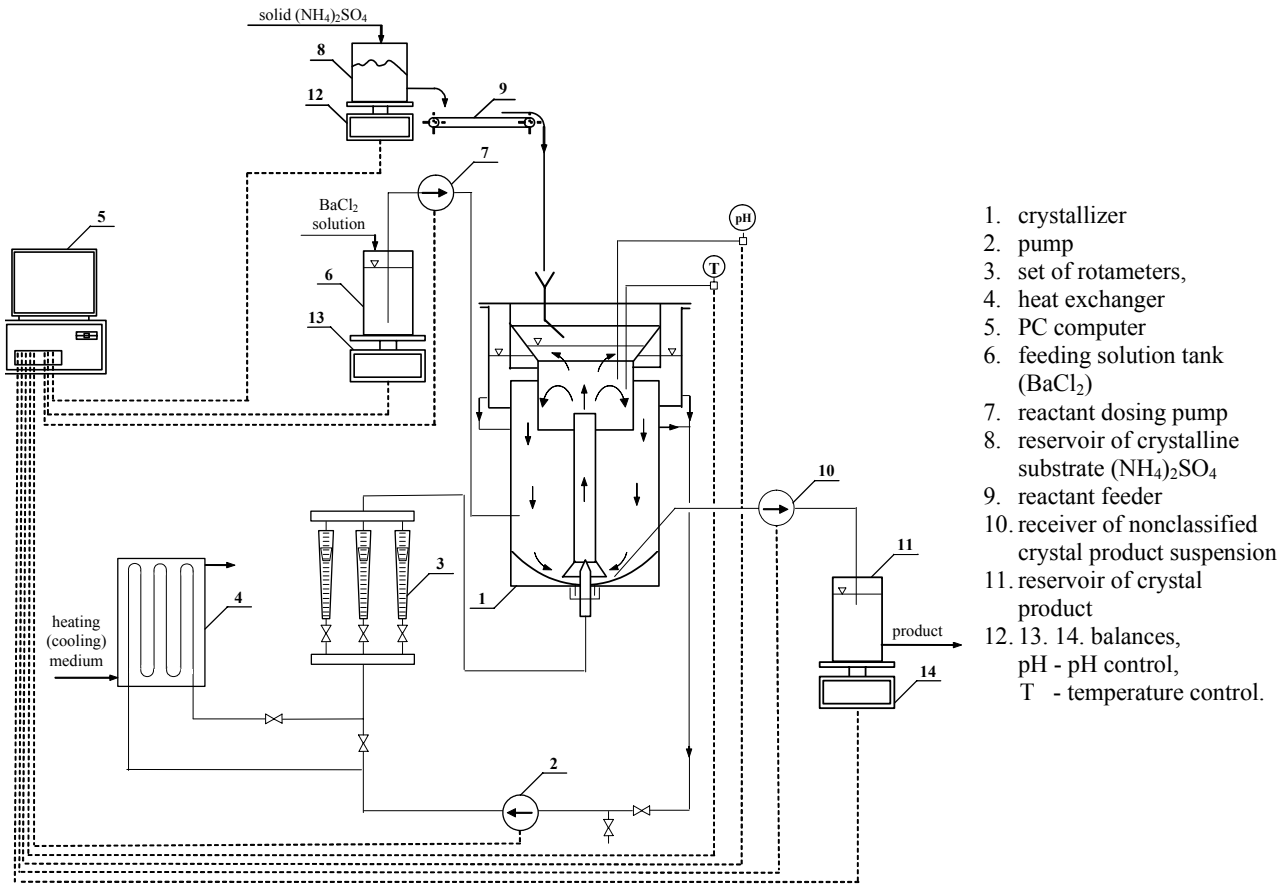

Figure 2: Scheme of the experimental stand with a DTM↑ crystallizer with a liquid jet-pump.

The crystallizers were provided with a water solution of barium chloride (after dissolution of $BaCl_2 \cdot 2H_2O$, p.a., POCh Gliwice, Poland, in distilled water) and, in stoichiometric proportions, with crystalline ammonium sulphate ($(NH_4)_2SO_4$ p.a., POCh Gliwice, Poland). Barium chloride solution was pumped into the so-called "crystal growth zone in the DTM and DT crystallizers" (a volume between the body of the crystallizer and a jet-pump device or a draft tube), while crystalline ammonium sulphate was dosed directly onto the free surface of the suspension. Feeding points of the reagents are visible in Fig. 1: (1) – $BaCl_2$ water solution, (2) – crystalline $(NH_4)_2SO_4$. Crystal suspension (not classified $BaSO_4$ product) was collected from the crystallizer bottom (3).

The measurements were performed at a fixed process temperature, T = 348 K, for the suspension residence time in the crystallizer vessel, τ = 900 s. Two concentrations of barium chloride in a feeding solution were tested: 10 and 24 mass % (barium chloride solubility in water at T = 293 K is 26.3 mass %, Mullin (1993)). The process parameter values applied to the model liquid jet-pump DTM constructions were selected purposefully in order to directly compare the results with the ones related to a DT-type "reference" crystallizer (Matynia et al., 2004; Matynia et al., 2005b) as well as for their potential practical application in the modern technology of proecological utilization of toxic quenching salts elaborated by the authors (Matynia, 2002). A continuous process of precipitation followed by integrated crystallization of barium sulphate was operated within the time of 5τ (measured from the moment of stabilization of the assumed conditions of pseudo-steady state). After this time the whole crystallizer content was withdrawn, cooled to room temperature, filtered and dried to be used in the CSD tests (laser particle analyzer COULTER LS – 230).

From the product crystal size distribution population density values, n_i, were calculated, Eq. (1):

$$n_i = \frac{m_i}{k_v \rho_c L_i^3 \Delta L_i V_w} = \frac{V_i}{k_v L_i^3 \Delta L_i V_w} \quad (1)$$

where m_i is the mass of the i^{th} crystal fraction, kg; V_i is the volume of the i^{th} crystal fraction, m^3; k_v is the crystal volumetric shape factor; ρ_c is the crystal density, kg m^{-3}; L_i is the average size of the i^{th} crystal fraction, m; ΔL_i is the size range of the i^{th} crystal fraction, m; and V_w is the crystallizer working volume, m^3.

Computed by this method the individual population density distributions of $BaSO_4$ crystals for the two $BaCl_2$ concentrations tested in the three model crystallizers are as shown in Fig. 3 and Fig. 4.

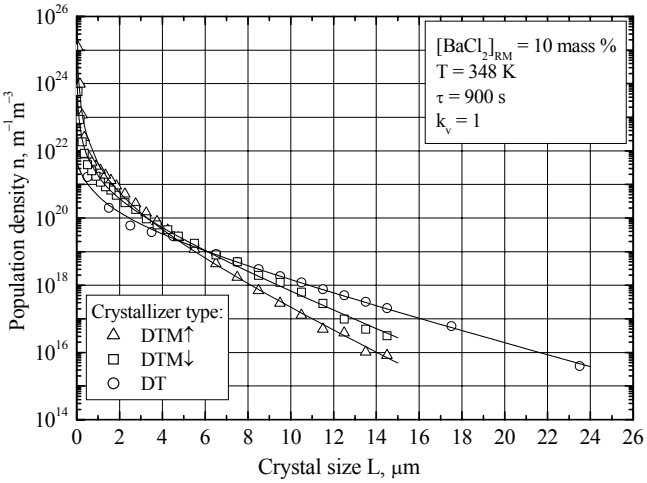

Figure 3: Comparison of population density distributions of barium sulphate crystals: points - experimental data, solid lines - values calculated with the use of Eq. (10) and data from Table 2 for the Rojkowski SDG hyperbolic model (RH).

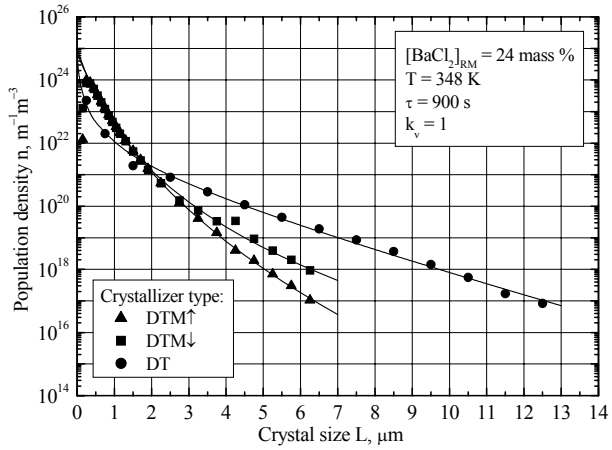

Figure 4: Comparison of population density distributions of barium sulphate crystals: points - experimental data, solid lines - values calculated with the use of Eq. (10) and data from Table 3 for the Rojkowski SDG hyperbolic model (RH).

Crystallization Kinetics

The law of preserving the crystal number is mathematically expressed in the population balance equation form (Mullin, 1993).

The population balance of the mass crystallization process enables one to evaluate the analytical (or – in more complex cases – numerical, solved with the use of advanced iterative algorithms) interdependence of the number (volume, mass) of crystals and their size in a form of CSD with the resulting final effect of interrelations between the intrinsic process kinetics, hydrodynamics, crystallizer construction, arrangement of the apparatus interior, decisive technological parameter values and presence of other accompanying processes. This function can also be practically interpreted as an essential indicator of crystal product quality.

For the basic, simplified mathematical model of a mass crystallization process, assuming steady state in the continuous crystallizer with ideally mixed content (suspension), withdrawal of nonclassified, representative product (MSMPR-type crystallizer) and the absence of any possible accompanying processes (e.g. attrition, breakage, agglomeration, dissolution, etc.) the crystal population balance equation can be formulated in the form of a simple differential equation (Randolph and Larson, 1988), Eq. (2):

$$-\frac{dn(L)}{n(L)} = \frac{dL}{G(L)\tau} + \frac{dG(L)}{G(L)} \tag{2}$$

where G is the crystal linear growth rate, m s^{-1} and τ is the suspension residence time, s.

From the experimental population density distributions ln(n) = f(L) of barium sulphate crystals (calculated from mass/volumetric CSD with the use of Eq. (1)), presented in Fig. 3 and Fig. 4, it can be observed that for the smallest size crystals (L < 2 μm) the distribution course is clearly concave on top. This can be interpreted as the presence in the system of a complex kinetic phenomenon – Size Dependent Growth (SDG). This observed behavior (sudden increase in the amount of fines) is very essential from practical point of view since within this size range the largest fraction of the number of crystals is located. Considering the fine-grained morphology, this fraction is characterized by the highest specific area in respect to the whole crystal population.

A more detailed description of the process kinetics – assuming the size-dependent growth (SDG) behavior and rendering the observed strong nonlinearity in the lnn(L) function for barium sulphate crystals of L < 2 μm (see Fig. 3 and Fig. 4) – requires adoption of some empirical form of G(L) dependency before solving Eq. (2).

The empirical or semiempirical G(L) equations taken under consideration were developed by Bransom (1960); Canning and Randolph (CR) (1967); Abegg, Stevens and Larson (ASL) (1968); Rojkowski: exponential model (RE) (Rojkowski, 1977), hyperbolic model (RH) (Rojkowski, 1978a) and hyperbolic II model (RHII) (Rojkowski, 1978b); Mydlarz and Jones (1990) and Mydlarz (1996). Detailed analysis of the mathematical construction and restrictions of these G = f(L) equations proved that the Bransom (1960), Mydlarz-Jones (1990) and Mydlarz (1996) equations are valid only for crystals of L > 0. The assumption that a zero-sized nucleus results in a zero growth rate from a mathematical point of view, makes its further growth impossible. This means that for practical application of these formulas it becomes necessary to arbitrarily assume that the nucleus has a specific – not more closely defined – size $L_z > 0$, which can introduce into the calculations some unpredictable calculation error.

Some solutions of Eq. (2), obtained in the form of n(L) analytical expressions, comply with the assumed G(L) forms and are presented below (Eq. (3–12)) (Piotrowski, 2002):

- ASL model (Abegg, Stevens and Larson, 1968):

$$G = G_0 (1 + aL)^b \tag{3}$$

for b = 1 $n = n_0 (1 + aL)^{-\left(\frac{1}{G_0 a\tau}+1\right)}$ (see Eq. (6))

for 0 < b < 1

$$n = n_0 \exp\left[-\left(\frac{1}{G_0 \tau a (1-b)}\left[(1+aL)^{1-b} - 1\right] + \frac{}{b \ln (1+aL)}\right)\right] \tag{4}$$

- CR model (Canning and Randolph, 1967):

$$G = G_0 (1 + aL) \tag{5}$$

$$n = n_0 (1 + aL)^{-\left(\frac{1}{G_0 a\tau}+1\right)} \tag{6}$$

- RE model (Rojkowski, 1977):

$$G = G_\infty - (G_\infty - G_0)\exp(-aL) \tag{7}$$

$$n = n_0 \exp\left[-\left(\frac{\ln\dfrac{G_\infty - (G_\infty - G_0)\exp(-aL)}{G_0}}{\left[\dfrac{1}{G_\infty a\tau}+1\right]+\dfrac{L}{G_\infty \tau}}\right)\right] \tag{8}$$

- RH model (Rojkowski, 1978a):

$$G = G_\infty - \left(\frac{G_\infty - G_0}{1+aL}\right) = \frac{G_0 + aG_\infty L}{1+aL} \tag{9}$$

$$n = n_0 \exp\left[-\left(\frac{1}{\tau}\frac{G_\infty - G_0}{aG_\infty^2}\ln\left(\frac{aG_\infty L + G_0}{G_0}\right) + \frac{1}{\tau}\frac{L}{G_\infty} + \ln\left(\frac{G_0 + aG_\infty L}{(1+aL)G_0}\right)\right)\right] \tag{10}$$

- RHII model (Rojkowski, 1978b):

$$G = \frac{G_0 G_\infty^2 \tau + G_\infty (G_\infty - G_0)L}{G_\infty^2 \tau + (G_\infty - G_0)L} \tag{11}$$

$$n = n_0 \exp\left[-\left(\ln\left(\frac{G_\infty(G_\infty - G_0)L + G_0 G_\infty^2 \tau}{G_0 G_\infty^2 \tau}\right) + \frac{L}{\tau G_\infty} + \ln\left(\frac{G_0 G_\infty^2 \tau + G_\infty (G_\infty - G_0)L}{\left[G_\infty^2 \tau G_0 + (G_\infty - G_0)LG_0\right]}\right)\right)\right] \tag{12}$$

where a is the parameter in the ASL, CR, RE and RH models of SDG, m^{-1}; b is the exponent in the ASL model of SDG; G is the crystal linear growth rate, m s^{-1}; G_0 is the minimum crystal linear growth rate (growth rate of nuclei), ms^{-1}; G_∞ is the maximum crystal linear growth rate, ms^{-1}; L is the characteristic linear size of the crystals, m; n is the population density (number of crystals within the specified size range in a unit volume of the suspension per this size range), $m^{-1}m^{-3}$; n_0 is the nuclei (zero-sized crystals) population density, $m^{-1}m^{-3}$ and τ is the suspension residence time, s.

Knowing the nuclei population density, n_0, and its linear growth rate, G_0, the nucleation rate B can then be calculated from the following simple relationship, Eq. (13):

$$B = n_0 G_0 \tag{13}$$

RESULTS AND DISCUSSION

On the basis of our experimental data (Fig. 3 and Fig. 4), using ORIGIN PRO 6.1 software (nonlinear regression tool), the following parameter n_0, G_0, G_∞, a and b values in the analytical relationships n(L) corresponding to the selected G(L) equations were computed. For each n(L) function (model) and each experimental data set a mean square deviation (variance – $(RMSD)^2$) was calculated in an ln form (see Eq. (14)):

$$(RMSD)^2 = \frac{\Sigma(\ln\ n^{calc}(L) - \ln\ n^{exp}(L))^2}{p-1} \tag{14}$$

where p is the number of experimental points.

A comparison of sums of variances $\Sigma(RMSD)^2$ for all six measurement series (see Table 1) enabled selection of the n(L) model which is the most compatible with our experimental data (assumed criterion – a minimal value of $\Sigma(RMSD)^2$) and thus the corresponding G(L) equation form.

Analysis of the sums of variance (Table 1) suggests that RH – the Rojkowski hyperbolic model with $\Sigma(RMSD)^2 = 0.4605$ – and RE – the Rojkowski exponential model with $\Sigma(RMSD)^2 = 0.7057$ – fit the experimental data well. These models render both steep curvature in the initial L range and apparent linearity within the remaining L range very well. The remaining models with their considerably higher $\Sigma(RMSD)^2$ values (ASL with $\Sigma(RMSD)^2 = 1.5064$, RHII with $\Sigma(RMSD)^2 = 1.6265$ and CR with $\Sigma(RMSD)^2 = 1.9397$) do not seem to be adequate for description of lnn(L) and G(L) relations in the system under study. The kinetic parameter values of the process run in DTM↑, DTM↓ and DT crystallizers, calculated by means of the five selected SDG models, are presented in Table 2 ($[BaCl_2]_{RM}$ = 10 mass %) and Table 3 ($[BaCl_2]_{RM}$ = 24 mass %).

Table 1: Barium sulphate reaction crystallization in DTM↑, DTM↓ and DT crystallizers - the $(RMSD)^2$ and $\Sigma(RMSD)^2$ values for the selected SDG models.

Crystallizer type	$[BaCl_2]_{RM}$ mass %	p	$(RMSD)^2$ for SDG model:				
			ASL	CR	RE	RH	RHII
DTM↑	10	27	0.5433	1.1403	0.1895	0.2097	0.3211
	24	24	0.0135	0.0123	0.0141	0.0132	0.2035
DTM↓	10	27	0.2603	0.6197	0.0630	0.0713	0.0824
	24	24	0.0558	0.0434	0.3613	0.0475	0.3852
DT	10	17	0.2927	0.0425	0.0288	0.0380	0.0740
	24	14	0.3408	0.0815	0.0490	0.0808	0.5603
$\Sigma(RMSD)^2$			1.5064	1.9397	0.7057	0.4605	1.6265

Explanations:
ASL - Abegg, Stevens and Larson model, Eqs. (3), (4) and (6)
CR - Canning-Randolph model, Eqs. (5) and (6)
RE - Rojkowski exponential model, Eqs. (7) and (8)
RH - Rojkowski hyperbolic model, Eqs. (9) and (10)
RHII - Rojkowski hyperbolic II model, Eqs. (11) and (12)

Table 2: Kinetic parameter values of nucleation and crystal growth for the selected SDG models in DTM↑, DTM↓ and DT-type crystallizers. Barium sulphate crystals obtained for barium chloride concentration in feeding solution 10 mass % at 348 K and τ = 900 s (k_v = 1).

Crystallizer type	SDG model	n_0	G_0	G_∞	a	b	B
–	–	$m^{-1}m^{-3}$	$m\ s^{-1}$	$m\ s^{-1}$	m^{-1}	–	$m^{-3}s^{-1}$
DTM↑	ASL	7.42×10^{26}	1.12×10^{-12}	–	25660097290	0.5951	8.34×10^{14}
	CR	1.12×10^{24}	1.70×10^{-10}	–	1367228	–	1.89×10^{14}
	RE	6.72×10^{26}	6.36×10^{-12}	1.32×10^{-9}	556534	–	4.28×10^{15}
	RH	8.10×10^{26}	5.24×10^{-12}	1.73×10^{-9}	471176	–	4.24×10^{15}
	RHII	8.79×10^{26}	2.72×10^{-12}	1.46×10^{-9}	–	–	2.39×10^{15}
DTM↓	ASL	2.75×10^{24}	1.63×10^{-11}	–	1206866602	0.5222	4.48×10^{13}
	CR	8.09×10^{22}	2.98×10^{-10}	–	899397	–	2.41×10^{13}
	RE	1.54×10^{24}	3.86×10^{-11}	1.59×10^{-9}	666537	–	5.95×10^{13}
	RH	3.13×10^{24}	2.40×10^{-11}	1.98×10^{-9}	634542	–	7.52×10^{13}
	RHII	2.96×10^{24}	2.85×10^{-11}	2.13×10^{-9}	–	–	8.44×10^{13}
DT	ASL	1.10×10^{21}	1.24×10^{-9}	–	311814	0.4807	1.36×10^{12}
	CR	4.85×10^{21}	7.48×10^{-10}	–	277298	–	3.63×10^{12}
	RE	4.93×10^{21}	4.47×10^{-10}	2.55×10^{-9}	378252	–	2.20×10^{12}
	RH	4.82×10^{21}	4.39×10^{-10}	3.00×10^{-9}	398064	–	2.12×10^{12}
	RHII	4.92×10^{21}	4.76×10^{-10}	3.23×10^{-9}	–	–	2.34×10^{12}

Table 3: Kinetic parameter values of nucleation and crystal growth for the selected SDG models in DTM↑, DTM↓ and DT-type crystallizers. Barium sulphate crystals obtained for barium chloride concentration in feeding solution 24 mass % at 348 K and τ = 900 s (k_v = 1).

Crystallizer type	SDG model	n_0	G_0	G_∞	a	b	B
		$m^{-1}m^{-3}$	$m\ s^{-1}$	$m\ s^{-1}$	m^{-1}	–	$m^{-3}s^{-1}$
DTM↑	ASL	6.94×10^{24}	1.86×10^{-10}	–	867275	0.7421	1.29×10^{15}
	CR	5.45×10^{24}	2.04×10^{-10}	–	448634	–	1.11×10^{15}
	RE	7.41×10^{24}	1.82×10^{-10}	1.18×10^{-9}	118908	–	1.35×10^{15}
	RH	6.87×10^{24}	1.87×10^{-10}	2.31×10^{-9}	53635	–	1.28×10^{15}
	RHII	7.43×10^{24}	1.26×10^{-10}	5.06×10^{-10}	–	–	9.36×10^{14}
DTM↓	ASL	9.43×10^{24}	1.48×10^{-10}	–	1841492	0.7574	1.39×10^{15}
	CR	8.13×10^{24}	1.63×10^{-10}	–	947614	–	1.32×10^{15}
	RE	9.05×10^{24}	1.56×10^{-10}	5.96×10^{-9}	28105	–	1.41×10^{15}
	RH	9.82×10^{24}	1.52×10^{-10}	6.87×10^{-9}	25304	–	1.49×10^{15}
	RHII	9.60×10^{24}	9.31×10^{-11}	6.34×10^{-10}	–	–	8.94×10^{14}
DT	ASL	6.40×10^{23}	1.82×10^{-10}	–	20442308	0.4041	1.17×10^{14}
	CR	1.49×10^{23}	5.03×10^{-10}	–	259525	–	7.51×10^{13}
	RE	5.63×10^{24}	5.99×10^{-11}	1.28×10^{-9}	660473	–	3.37×10^{14}
	RH	5.39×10^{24}	5.64×10^{-11}	1.57×10^{-9}	649477	–	3.04×10^{14}
	RHII	5.35×10^{24}	5.42×10^{-11}	1.54×10^{-9}	–	–	2.90×10^{14}

Population density plots of the experimental data are presented in Fig. 3 ($[BaCl_2]_{RM}$ = 10 mass %) and Fig. 4 ($[BaCl_2]_{RM}$ = 24 mass %). From Fig. 3 it can be concluded that for L larger than ca. 8 μm the effect of particle size on linear growth rate G is less and less pronounced, which is graphically represented by transformation of the distinctly observed curvature of lnn(L) within the initial L range into a practically linear relationship. Similar conclusions can be drawn from Fig. 4, but only for a DT apparatus where the authors have more n(L) data at their disposal than in the case of both liquid jet-pump DTM crystallizers. This experimental trend, observed in Fig. 3 and Fig. 4, is also reflected in Fig. 5 presenting the resulting six G(L) dependency courses for the three crystallizers and two assumed $BaCl_2$ concentrations analyzed in this study (the linear course of lnn(L) in Figs. 4 and 5 corresponds to stabilization of G value in Fig. 5 and thus its independence of L).

From Fig. 5 it can be concluded that for $[BaCl_2]_{RM}$ = 10 mass % the highest value of G corresponds to a DT-type crystallizer ($G_0 = 4.39\times10^{-10}$ m s^{-1} and $G_\infty = 3.00\times10^{-9}$ m s^{-1}). Table 2 informs also that higher G corresponds to the DTM↓ type ($G_0 = 2.40\times10^{-11}$ m s^{-1} and $G_\infty = 1.98\times10^{-9}$ m s^{-1}) rather than to the DTM↑construction ($G_0 = 5.24\times10^{-12}$ m s^{-1} and $G_\infty = 1.73\times10^{-9}$ m s^{-1}). It is noticeable that the difference between asymptotic values of G_∞ for DTM↓ ($G_\infty = 1.98\times10^{-9}$ m s^{-1}) and DTM↑ ($G_\infty = 1.73\times10^{-9}$ m s^{-1}) is rather small. This important observation can be interpretted theoretically by calling attention of the reader to the hydrodynamic regime of inner circulation and the specific method of contacting both reagents in this original technology. Both constructions, DT and DTM↓, are characterized by a descending flow of suspension in the circulation profile/device. In this specific reaction crystallization system, a key factor in the instant ionic reactions in water solution seems to be a dissolution rate of the solid reagent, $(NH_4)_2SO_4$, being in turn a function of hydrodynamic conditions and turbulence level on micro- and macroscale within the bulk solution. As can be expected, the DTM↑ construction, with rather mild mixing conditions during ascending flow of circulated medium (e.g. final "fountain phenomenon" with a minimum of kinetic energy) provides in effect the lowest values of G. This dissolution phenomenon is also indirectly coupled with another kinetic process – nucleation rate. Lower dissolution rates (in a DT → DTM↓ → DTM↑order), as the effect of mixing that is not intensive enough, are also responsible for the lower efficiency in discharging the resulting concentration into the bulk of surrounding mother solution. In effect it can be presumed that some adhesive film layer of highly supersaturated mother liquid is spontaneously formed on the surface of the $(NH_4)_2SO_4$ substrate, where a higher nucleation (heterogeneous or even homogeneous) rate can be observed (possible catalytic effect of the ammonium sulphate surface, crystalographically similar to a product barium sulphate crystal network – catalytic/induced nucleation). The SDG model calculations also confirm these theoretical considerations, since for the DT-type apparatus the nucleation rate is B = 2.12×10^{12} m^{-3}s^{-1}, for DTM↓ it is B = 7.52×10^{13} m^{-3}s^{-1} and finally for DTM↑ it reaches the highest value, B = 4.24×10^{15} m^{-3}s^{-1}.

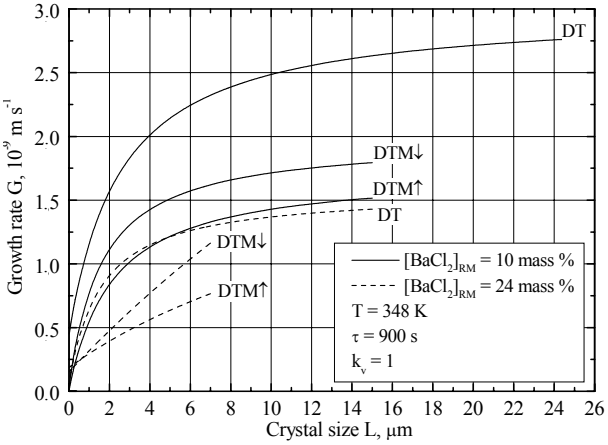

Figure 5: Dependence of linear growth rate of barium sulphate crystals on their size G(L) - Eq. (9) - and data from Table 2 and Table 3 - application of Rojkowski SDG hyperbolic model (RH).

A higher concentration of $BaCl_2$ in feeding solution ($[BaCl_2]_{RM}$ = 24 mass %, Table 3) corresponds to a noticeable modification of overall (diffusion mechanism coupled with convection) mass transfer conditions between mother solution and suspended crystal phase. In this case the highest value of G_∞ corresponds to a DTM↓ construction ($G_\infty = 6.87\times10^{-9}$ m s^{-1}, while $G_0 = 1.52\times10^{-10}$ m s^{-1}). A similar construction, DTM↑, has a bit lower value of maximal growth rate ($G_\infty = 2.31\times10^{-9}$ m s^{-1}, while $G_0 = 1.87\times10^{-10}$ m s^{-1}), roughly comparable with the value corresponding to a DT design ($G_\infty = 1.57\times10^{-9}$ m s^{-1}, while $G_0 = 5.64\times10^{-11}$ m s^{-1}). In the case of nucleation rate, similar values of B parameter are obtained for both jet-pump constructions, B = 1.49×10^{15} m^{-3}s^{-1} for DTM↓ and B = 1.28×10^{15} m^{-3}s^{-1} for DTM↑), while for the DT apparatus the B value is considerably lower (B = 3.04×10^{14} m^{-3}s^{-1}).

It can be concluded that from a technological point of view with the increase in $BaCl_2$ concentration (from 10 to 24 mass %) in the case of the DT construction disadvantageous tendency is observed – a decrease in linear growth rate (G_∞ from 3.00×10^{-9} m s^{-1} to 1.57×10^{-9} m s^{-1} and G_0 from 4.39×10^{-10} m s^{-1} to 5.64×10^{-11} m s^{-1}) coupled with a considerable increase in nucleation rate B (from 2.12×10^{12} m^{-3}s^{-1} to 3.04×10^{14} m^{-3}s^{-1}).

In the case of the DTM↓ apparatus, in spite of a significant increase in B value from 7.52×10^{13} m^{-3}s^{-1} to 1.49×10^{15} m^{-3}s^{-1} (however, the increment is smaller than in the DT case) an advantageous improvement in growth rate kinetics is observed (an increase in G_∞ from 1.98×10^{-9} m s^{-1} to 6.87×10^{-9} m s^{-1} coupled with a simultaneous increase in G_0 from 2.40×10^{-11} m s^{-1} to 1.52×10^{-10} m s^{-1}).

Comparing the data for the DTM↑ crystallizer it is concluded that a slight increase in the G_∞ parameter value (from 1.73×10^{-9} m s^{-1} to 2.31×10^{-9} m s^{-1}) and a noticeable increase in G_0 (from 5.24×10^{-12} m s^{-1} to 1.87×10^{-10} m s^{-1}) correspond to an advantageous, however limited, decrease in nucleation rate (from B = 4.24×10^{15} m^{-3}s^{-1} to 1.28×10^{15} m^{-3}s^{-1}).

Similar conclusions come to mind in analyzing the kinetic parameter values provided by a second SDG equation, namely the Rojkowski exponential (RE) model, with a bit lower statistical quality to the experimental data ($\Sigma(RMSD)^2 = 0.7057$ for the RE model compared to $\Sigma(RMSD)^2 = 0.4605$ for the RH model discussed here in detail – see Table 1).

For example, in the case of a lower concentration of $BaCl_2$ (10 mass %, Table 2) it is observed that for the DTM↑ crystallizer $G_0 = 5.24\times10^{-12}$ m s^{-1} (RH) and 6.36×10^{-12} m s^{-1} (RE), $G_\infty = 1.73\times10^{-9}$ m s^{-1} (RH) and 1.32×10^{-9} m s^{-1} (RE) and B = 4.24×10^{15} m^{-3}s^{-1} (RH) and 4.28×10^{15} m^{-3}s^{-1} (RE). For the DTM↓ crystallizer the corresponding kinetic parameter values are as follows: $G_0 = 2.40\times10^{-11}$ m s^{-1} (RH) and 3.86×10^{-11} m s^{-1} (RE), $G_\infty = 1.98\times10^{-9}$ m s^{-1} (RH) and 1.59×10^{-9} m s^{-1} (RE) and B = 7.52×10^{13} m^{-3}s^{-1} (RH) and B = 5.95×10^{13} m^{-3}s^{-1} (RE). Finally, in the case of the DT type apparatus the data are $G_0 = 4.39\times10^{-10}$ m s^{-1} (RH) and 4.47×10^{-10} m s^{-1} (RE), $G_\infty = 3.00\times10^{-9}$ m s^{-1} (RH) and 2.55×10^{-9} m s^{-1} (RE) and B = 2.12×10^{12} m^{-3}s^{-1} (RH) and 2.20×10^{12} m^{-3}s^{-1} (RE).

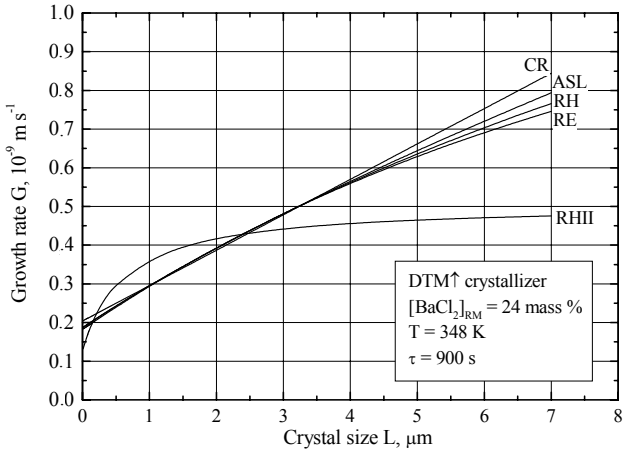

Figure 6: Dependence of linear growth rate of barium sulphate crystals on their size in the DTM↑ crystallizer – Eqs. (3), (5), (7), (9) and (11) with kinetic data from Table 3.

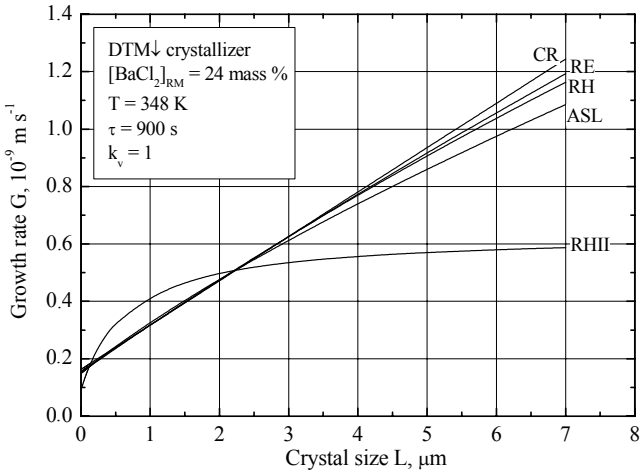

Figure 7: Dependence of linear growth rate of barium sulphate crystals on their size in the DTM↓ crystallizer – Eqs. (3), (5), (7), (9) and (11) with kinetic data from Table 3.

Similar observations can be made on the basis of Table 3. In Fig. 6 and Fig. 7, coincidence of G(L) curves provided by the RH and RE SDG models is clearly observed. Since their statistical indicators $\Sigma(RMSD)^2$ are considerably higher (within the 1.5064 – 1.9397 range), all remaining SDG models (ASL, CR, RHII) provide kinetic data not strictly compatible with the experimental data. This results mainly from the mathematical limitations of the model equations, an inability to adjust to the characteristic curve of population density of experimental data characterized by both pronounced, high curvature within the range of smaller sizes and linearity for the largest sizes (flexibility of modeling). However, all these kinetic data (five SDG models – see Table 2 and Table 3) are quantitatively similar, in each case differing from each other maximally by one order of magnitude (except the CR and RHII sets – see also Fig. 6 and Fig. 7).

CONCLUSIONS

Two laboratory model crystallizers with internal circulation of suspension were tested in respect to their practical applicability in the area of reaction crystallization processes during precipitation of sparingly soluble inorganic compounds. An original liquid jet-pump construction was used in them (DTM↓ and DTM↑) to secure the stable and sufficiently intensive circulation of growing crystal magma. The results were also compared with those for a conventional "reference" crystallizer equipped with a propeller agitator and a draft tube (DT) profile. The subject of process research was an original proecological technology, where reaction crystallization of $BaSO_4$ was practically controlled by dissolution rate of solid substrate $(NH_4)_2SO_4$. Thus, in this specific process environment the hydrodynamic conditions (macro- and micromixing effects) inside the apparatus vessel (resulting, in turn, from the geometrical arrangement and its operational mode) played an extremely important role.

On the basis of research results for this specific system (highly concentrated solutions of $BaCl_2$ contacted with solid $(NH_4)_2SO_4$), it can be concluded that with a gradual increase in a $BaCl_2$ concentration in the feeding solution (from 10 to 24 mass %) the initial superiority of the DT constructional solution over the two other designs (DTM↓ and DTM↑), characterized by higher values of linear growth rates (both minimal and maximal) coupled with a lower nucleation rate, is beginning to yield to the advantages of modern liquid jet-pump constructions. In this case (24 mass % concentration) higher values of linear growth rate are observed in the DTM↓ and DTM↑crystallizers, for both the G_0 and G_∞ parameters. Analyzing the nucleation data in connection with growth kinetic characteristics, however, one can conclude that although in the jet-pump construction nucleation rate is ca. one magnitude higher than that in the DT reference data, simultaneously higher values of both nucleation and growth rate indicate a general considerable improvement in the conditions of mass transfer between supersaturated mother solution and growing crystal phase.

The experimental data presented can be practically applied for improving the construction of liquid jet-pump DTM crystallizers recommended for

reaction crystallization of sparingly soluble inorganic salts (especially for high concentrations of reaction substrates) in modern industrial-scale technologies.

ACKNOWLEDGEMENT

Crystal size distributions of barium sulphate were measured by means of a particle size analyzer COULTER LS – 230 at the Institute of Inorganic Chemistry, Gliwice, Poland.

NOMENCLATURE

a	parameter in ASL, CR, RE and RH models of SDG	m^{-1}
b	exponent in ASL model of SDG	
B	nucleation rate	$m^{-3}s^{-1}$
$[BaCl_2]_{RM}$	concentration of barium chloride in the crystallizer feeding solution	mass %
G	crystal linear growth rate	m s^{-1}
G_0	minimal crystal linear growth rate (growth rate of nuclei)	m s^{-1}
G_∞	maximal crystal linear growth rate	m s^{-1}
k_v	crystal volumetric shape factor	(-)
L	characteristic linear size of crystal	m
L_i	average size of i^{th} crystal fraction in Eq. (1)	m
L_z	nucleus size	m
ΔL_i	size range of i^{th} crystal fraction in Eq. (1)	m
m_i	mass of i^{th} crystal fraction in Eq. (1)	kg
n	population density (number of crystals within the specified size range in a unit volume of the suspension per this size range)	$m^{-1}m^{-3}$
n_i	population density of i^{th} crystal fraction in Eq. (1)	$m^{-1}m^{-3}$
n_0	nuclei (zero–sized crystals) population density	$m^{-1}m^{-3}$
n^{calc}	population density calculated	$m^{-1}m^{-3}$
n^{exp}	population density experimental	$m^{-1}m^{-3}$
P_{eu}	unit power of feeding stream	W kg^{-1}
p	number of experimental points	
q_{vs}	volumetric flow rate of suspension	m^3 s^{-1}
s	number of agitator revolutions	s^{-1}
T	process temperature	K
V_i	volume of i^{th} crystal fraction in Eq. (1)	m^3
V_w	crystallizer working volume	m^3

Greek Letters

ρ_c	crystal density	kg m^{-3}
τ	suspension residence time	$\tau=V_w/q_{vs}$ s

Abbreviations

ASL	Abegg, Stevens and Larson model of SDG	(-)
CR	Canning and Randolph model of SDG	(-)
CSD	Crystal Size Distribution	(-)
DT	Draft Tube (crystallizer)	(-)
DTM	Draft Tube Magma (crystallizer)	(-)
MSMPR	Mixed Suspension Mixed Product Removal (crystallizer)	(-)
RE	Rojkowski exponential model of SDG	(-)
RH	Rojkowski hyperbolic model of SDG	(-)
RHII	Rojkowski hyperbolic II model of SDG	(-)
RMSD	Root Mean Square Deviation (in this work calculated in an ln form)	(-)
$(RMSD)^2$	Mean Square Deviation (variance) (in this work calculated in an ln form)	(-)
SDG	Size-dependent Growth	(-)

REFERENCES

Abegg, C.F., Stevens, J.D. and Larson, M.A., Crystal Size Distributions in Continuous Crystallizers When Growth Rate is Size Dependent, AIChE J., 14, 118 (1968).

Bransom, S. H., Factors in the Design of Continuous Crystallizers, Brit. Chem. Eng., 5, 838 (1960).

Canning, T. F. and Randolph, A. D., Some Aspects of Crystallization Theory: Systems that Violate McCabe's Delta L Law, AIChE J., 13, 5 (1967).

Koralewska, J., Matynia, A., Piotrowski, K. and Wierzbowska, B., Crystallization of Barium Sulphate in a Continuous DTM Type Crystallizer with a Jet-Pump of Descending Suspension Flow in a Mixing Chamber, Materials of the International Congress of Chemical and Process Engineering CHISA, CD–ROM, No. 278, Proc. Eng. Publisher, Prague, Czech Republic (2006a).

Koralewska, J., Matynia, A., Piotrowski, K. and Wierzbowska, B., Precipitation of Barium Ions with Solid Ammonium Sulfate in a Continuous DTM Crystallizer with a Liquid Jet Pump of Ascending Suspension Flow in a Mixing Chamber, Chem. Proc. Eng., 27, 1555-1579 (2006b).

Matynia, A., Crystallizers with a Jet-Pump, Inż. Ap. Chem., 36, No. 6, 9 (1997) (in Polish).

Matynia, A., Wlazło, P. and Koralewska, J., The Influence of Residence Time on the Crystallization of Barium Sulphate in the Process of Barium Ions Precipitation by Means of Crystalline Ammonium Sulphate Addition, Pol. J. Appl. Chem., XLV, No. 3-4, 91 (2001).

Matynia, A., Used Quenching Salts Treatment Process, Environ. Protection Eng., 28, No. 2, 77 (2002).

Matynia, A., Piotrowski, K., Koralewska, J. and Wierzbowska, B., Barium Sulphate Crystallization Kinetics in the Used Quenching Salts Treatment Process, Chem. Eng. Technol., 27, 559 (2004).

Matynia, A., Koralewska, J., Wierzbowska, B. and Piotrowski, K., Jet-Pump Crystallizers in the Reaction-Crystallization Processes of Sparingly Soluble Salts, Pol. J. Chem. Technol., 7, No. 3, 56 (2005a).

Matynia, A., Piotrowski, K. and Koralewska, J., Barium Sulphate Crystallization Kinetics in the Process of Barium Ions Precipitation by Means of Crystalline Ammonium Sulphate Addition, Chem. Eng. Proc., 44, 485 (2005b).

Mersmann, A., Crystallization Technology Handbook, Marcel Dekker, New York (1995).

Mullin, J.W., Crystallization, Butterworth–Heinemann, Oxford (1993).

Mydlarz, J. and Jones, A. G., On Modelling the Size-Dependent Growth Rate of Potassium Sulphate in a MSMPR Crystallizer, Chem. Eng. Comm., 90, 47 (1990).

Mydlarz, J., A Hyperbolic Crystal Growth Rate Model, 13th Symposium on Industrial Crystallization, Toulouse, 275 (1996).

Myerson, A.S., Handbook of Industrial Crystallization, Butterworth-Heinemann, Boston (1993).

Nielsen, A.E., Kinetics of Precipitation, Pergamon Press, Oxford (1964).

Nývlt, J., Söhnel, O., Matuchová, M. and Broul, M., The Kinetics of Industrial Crystallization, Academia, Prague (1985).

Piotrowski, K., Computer Aided Design of Continuous Tank Crystallizers, Ph.D. diss., Silesian University of Technology, Gliwice, Poland (2002) (in Polish).

Randolph, A. D. and Larson, M. A., Theory of Particulate Processes: Analysis and Techniques of Continuous Crystallization, Academia Press, New York (1988).

Rojkowski, Z., New Empirical Kinetic Equation of Size Dependent Crystal Growth and Its Use, Kristall und Technik, 12, 1121 (1977).

Rojkowski, Z., New Hyperbolic Empirical Model of Size Dependent Crystal Growth, Bulletin de L'Academie Polonaise des Sciences - Serie des sciences chimiques, XXVI, 265 (1978a).

Rojkowski, Z., Two Parameter Kinetic Equation of Size Dependent Crystal Growth, Kristall und Technik, 13, 1277 (1978b).

Rojkowski, Z. and Synowiec, J., Krystalizacja i Krystalizatory, WNT, Warsaw (1991) (in Polish).

Sőhnel, O. and Garside, J., Precipitation: Basic Principles and Industrial Applications, Butterworth-Heinemann, Boston (1993).